ELSEVIER

Astroparticle Physics 10 (1999) 291–302

Astroparticle Physics

The cosmic ray energy spectrum between 10^{14} and 10^{16} eV

M.A.K. Glasmacher [a], M.A. Catanese [a,1], M.C. Chantell [b], C.E. Covault [b], J.W. Cronin [b], B.E. Fick [b], L.F. Fortson [b,2], J.W. Fowler [b], K.D Green [b,3], D.B. Kieda [c], J. Matthews [a,*], B.J. Newport [b,4], D.F. Nitz [a,5], R.A. Ong [b], S. Oser [b], D. Sinclair [a], J.C. van der Velde [a]

[a] *Dept. of Physics, The University of Michigan, Ann Arbor, MI 48109, USA*
[b] *Enrico Fermi Institute, The University of Chicago, Chicago, IL 60637, USA*
[c] *Dept. of Physics, The University of Utah, Salt Lake City, UT 84112, USA*

Received 27 August 1998; revised 26 November 1998; accepted 4 December 1998

Abstract

The energy spectrum of cosmic rays with primary energies between 10^{14} eV and 10^{16} eV has been studied with the CASA-MIA air shower array. The measured differential energy spectrum is a power law ($dj/dE \propto E^{-\gamma}$) with spectral indices γ of 2.66 ± 0.02 below approximately 10^{15} eV and 3.00 ± 0.05 above. A new method is used for measuring primary energy derived from ground-based data in a compositionally insensitive way. In contrast with some previous reports, the "knee" of the energy spectrum does not appear sharp, but rather a smooth transition over energies from 10^{15} eV to 3.0×10^{15} eV. © 1999 Elsevier Science B.V.

1. Introduction

Over 80 years after the initial discovery of cosmic rays, their source and acceleration mechanism are still not fully understood. Currently, supernovae are the most favored candidate sources for lower energy cosmic rays. The upper limit of acceleration expected from supernovae, however, is in the range of 10^{14} to 10^{15} eV in most models. Cosmic rays have been observed with energies much higher than this – up to over 10^{20} eV. Clearly, supernova acceleration, at least as it is currently understood, cannot be used to explain the entire range of cosmic ray energies.

The energy spectrum of cosmic rays can be a very useful tool for probing their origin and acceleration mechanism. Existing models make predictions about the cosmic ray spectrum which can be compared to observations. The spectrum has been previously observed by many ground-based experiments to resemble two power laws, having a form $dj/dE \propto E^{-\gamma}$, with $\gamma = 2.7$ below about $10^{15.5}$ eV, and then steepening to $\gamma = 3.1$ above this energy [1]. The change in the spectrum at around $10^{15.5}$ eV, called the spectral "knee", occurs near the maximum energy attainable from supernova acceleration, inviting the suggestion

* Corresponding author. Current address: Dept. of Physics and Astronomy, Louisiana State University, Baton Rouge, LA 70803 and Dept. of Physics, Southern University, Baton Rouge, LA 70801, USA.

[1] Current address: Dept. of Physics and Astronomy, Iowa State University, Ames, IA 50011, USA.

[2] Joint appointment with The Adler Planetarium and Astronomy Museum, Astronomy Department, Chicago, Illinois 60605, USA.

[3] Current address: Koch Industries, Wichita, KS 67201, USA.

[4] Current address: Micro Encoder, Inc., Kirkland, WA 98034, USA.

[5] Current address: Dept. of Physics, Michigan Technological University, Houghton, MI 49931, USA.

0927-6505/99/$ - see front matter
PII S0927-6505(98)00070-X

that the break is related to this limit. Another possibility is that the "knee" is formed as cosmic rays attain enough energy to escape the Galaxy. Again, a bend in the spectrum is expected, at an energy determined by the strength and geometry of the Galactic magnetic field. The energy is coincidentally quite similar to the maximum energy available from supernovae shock wave acceleration.

One difficulty with the models, however, is that they do not well reproduce the experimentally observed knee, which appears to be rather abrupt, i.e., the change in the spectral index occurs over a small range of energies. The knee was first reported as an anomaly in the spectrum of electron sizes of air showers by the Moscow group [2]. Since that result, there have been many confirmations of the effect, both in the electron size spectrum and in the energy spectrum. The most recent experimental results have been well summarized by Watson [3]; eight of nine experiments report a rather sudden spectral steepening in the range $2–6 \times 10^{15}$ eV, with only the Tibet Air Shower Array exhibiting a smooth transition in this energy range [4].

Ground-based experiments typically infer the energy spectrum in one of two ways. In one method, electron sizes are measured and then the energy spectrum is calculated from a simulation-based correspondence formula. Another technique uses optical measurements of Čerenkov or fluorescence light from showers, providing a more calorimetric determination of the energy. The latter method is presumed to be more insensitive to assumptions about the primary composition. The electron size-energy technique must assume some specific mixture of primary nuclei in the calculation. If the assumed composition is taken as unchanging, then the shape of the energy spectrum will be identical to that of the measured electron size spectrum. The work reported here uses a new combination of electron and muon sizes which will be shown to be insensitive to the type of primary particle.

A sharp spectral change in the primary energy spectrum is difficult to produce with most cosmic ray models. Some have proposed that detector effects may be responsible for the observed sharpness of the knee, or perhaps cause it entirely. The Akeno group has published a very sharp knee feature [5], but have recently discussed systematic trigger and reconstruction effects which may influence the observation [6]. Several large ground-array experiments (EAS-TOP [7], KASCADE [8], and HEGRA [9]) have recently given energy spectra measurements with intensities which are in reasonably good agreement with the Tibet experiment, except for knee features which are sharper to varying degrees. Note that the Tibet group uses a technique which, while measuring shower particles at the ground, is nevertheless fairly insensitive to the nuclear composition of the primary cosmic rays, as will be further discussed below. HEGRA, using optical measurements, reports a fairly sharp knee in two separate analyses, but these two results are not entirely in agreement with each other [3].

It will be shown here that the CASA-MIA detector also observes a cosmic ray *energy* spectrum with a smooth knee, while recording a *size* spectrum with a sharper spectral change. This suggests compositional and detector effects which may have been the cause of the sharp knee observed in other experiments. In the present CASA-MIA results, the energy has been derived in a compositionally insensitive way, and is therefore free of the biases present in many previous measurements.

2. The CASA-MIA detector

The CASA-MIA detector (more thoroughly described elsewhere [10]) is a ground-based array of 1089 surface particle detectors (CASA) and 1024 underground muon detectors (MIA) located at the Dugway Proving Grounds southwest of Salt Lake City, Utah. The mean atmospheric overburden is 870 g cm^{-2}. The layout is shown in Fig. 1.

The squares in Fig. 1 represent the CASA detector stations. Each station contains four counters, each of which consists of a two inch diameter photomultiplier tube glued to a square sheet of acrylic scintillator 61 cm on a side and 1.5 cm thick, wrapped in a black plastic tray. Each station has a thin (1 radiation length) lead sheet on its top, which converts some of the photons in the air shower, resulting in a net increase of the scintillator signal.

The CASA stations are spaced 15 m apart on a square grid and connected to each of their four neighbors by timing cables. The array triggers when any three stations report at least three hit counters each. Stations with two or more counters reporting hits are "alerted" and digitize and store their data.

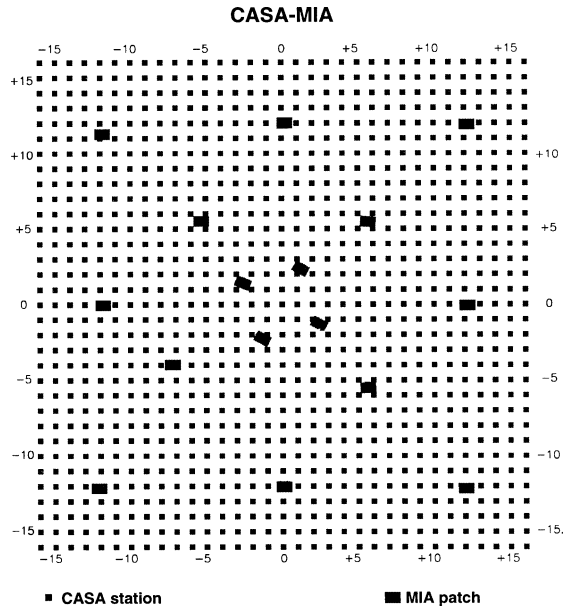

Fig. 1. The layout of the CASA-MIA array. CASA is on the surface, and MIA is buried 3 meters underground. The CASA stations are 15 meters apart.

The MIA counters are arranged in 16 patches, each of which contains 64 individual counters. Each counter is a 1.6 m by 1.9 m sheet of acrylic scintillator viewed by one 5 inch diameter photomultiplier tube. The MIA patches are buried 3 meters underground and so register muons with energies exceeding about 750 MeV at the surface. Electromagnetic punch-through to the muon counters is negligible in comparison to the muon signal.

The data acquired are processed through a series of fits to determine the direction, core location, "electron size" (N_{e*}) and muon size (N_μ), among other quantities, of the shower. The subscript "e*" is used here to emphasize that, strictly speaking, the quantity N_{e*} does not simply represent the number of electrons above some threshold energy, but includes a fraction of shower photons and positrons as well (see Section 6). The sizes are obtained by fitting either an Nishimura–Kamata–Greisen (NKG) [11] function (for surface data) or a Greisen function [12] (for underground data) to the observed particle densities as they diminish with distance from the shower core.

Descriptions of the detector, its calibrations, and the standard fits have been previously published [10].

3. Data

Several strict selection cuts are employed in the present analysis to ensure the integrity of the data. First, for vertical spectra, no events were accepted which arrived more than 14° from the zenith. (Specifically, the cut requires that $\cos\theta > 0.97$; spectra at angles other than vertical are examined separately, in bins of equal cosine of the zenith angle.) This angular range corresponds to a systematic deviation in shower size of about 3% between showers of a given energy arriving from vertical and those at the maximum zenith angle allowed (14°). Second, to avoid the effects of the edge of the array, only events which fall within a square 300 m on a side, centered in the array, are used. Third, events for which any one of the fitting routines (core location, direction, size) failed are rejected as well.

After these cuts are performed, 54 million events remain for use in studying the vertical spectrum. These represent a live-time equivalent to 342 days of continuous running.

4. Simulation

An air shower simulation is necessary to connect the measurements of air shower properties at the ground with the properties of the initiating cosmic ray primary. The MOCCA [13] shower simulation program, using the SIBYLL [14] hadron interaction codes, was chosen here for this purpose. An E^{-1} differential spectrum of over one thousand iron and one thousand proton showers of energies between 10^{13} and $10^{16.5}$ eV was generated. To conserve computing time, the algorithm employs a technique called *thinning*, where air shower particles are only selectively tracked when their energies are below 10 GeV (100 GeV), in showers whose primary energy was less than (greater than) 10^{16} eV.

The simulated air shower particles are then processed through a simulated detector to account for the effects of particle detection, the array trigger, and the electronics. The detector simulation followed the particles in as much detail as possible – statistically covering the steps from the deposit of energy in the scintillator to the generation of a signal from the photomultiplier, including time slewing. After running through the detector calibration and triggering procedures, the

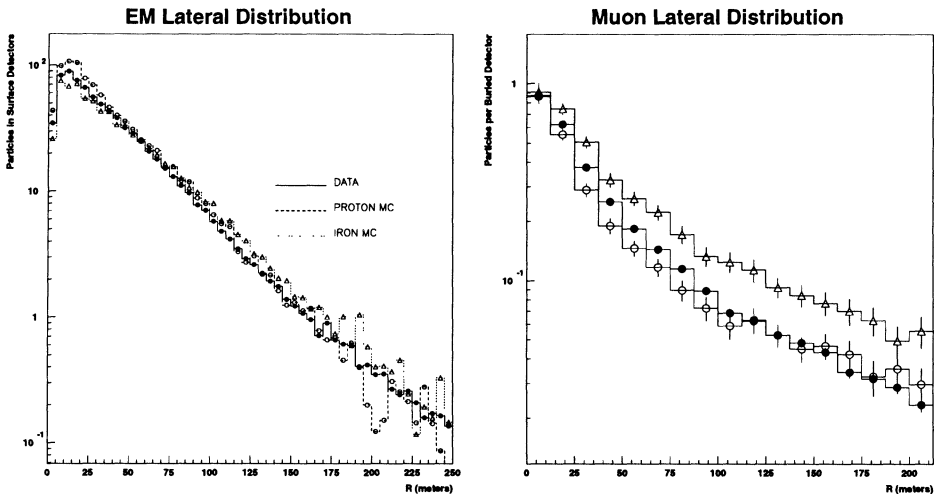

Fig. 2. Comparisons of the distributions of surface and underground particles for the simulation (○ – protons, △ – iron) to data (●). These distributions for showers with more than 60 and less than 200 alerts are averaged. The simulation showers are weighted to correct their flat spectrum to the observed cosmic ray spectrum.

simulated showers closely resembled real data showers, enabling the use of the same set of reconstruction codes that are used on actual data. The resulting core location, shower direction, and shower sizes are then retained for further analysis.

Fig. 2 compares the electron and muon lateral distributions obtained from the data to those from the simulated iron and proton showers. In both cases, the data lie between the "extremes" of iron and protons, giving confidence that the simulation is accurately representing the data. Many other comparisons have been made which show good agreement between the data and simulation [15], including examination of quantities such as the arrival times of particles at the ground, the shape of the shower front, and the distributions of alerted and triggered surface stations.

5. Energy determination

The sensitivity of measurements of electron size at the ground to the nuclear species of the primary cosmic ray has been a potential problem for previous composition measurements. However, using the muon information available from CASA-MIA, a good measurement of the energy which is not dependent on the underlying nuclear composition can be obtained.

The bulk of the energy of the primary cosmic ray is dissipated through ionization losses of the particles in the resulting air shower. This energy loss is roughly proportional to the primary energy. The remaining energy (also proportional to the primary energy) reaches the ground in the form of kinetic energy of individual particles, divided mainly between the electromagnetic portion (electrons, positrons, and photons) and the muons and neutrinos from hadronic interactions. CASA-MIA measures a significant portion of this energy, missing only the neutrinos.

It might be expected that a suitable combination of the number of muons and the number of electrons at ground level will give a quantity that is simply related to the primary energy and independent of the type of primary particle. The number of muons in showers from heavy nuclei is greater than that from proton showers (at the same primary energy), but the number of electrons is less. The latter effect is due both to less of the shower energy flowing into electromagnetic channels as well as more rapid attenuation of the electron and photon numbers with depth after shower maximum. The shower maximum is higher in the atmosphere for heavy primaries.

Fig. 3 shows the empirically determined optimal value of the energy parameterization ($N_{e*}+60\times N_{\mu}$) as a function of energy, for two sets of vertical simulation showers, one purely protons and the other all iron. N_{e*} and N_{μ} are obtained from the standard fits of

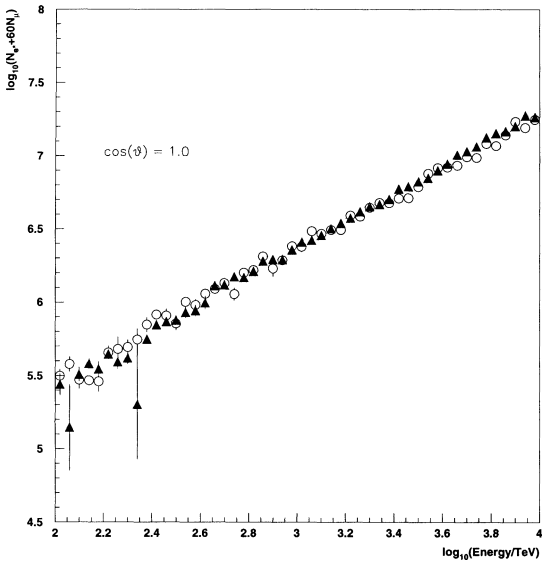

Fig. 3. The energy parameter $\log_{10}(N_{e*} + 60 \times N_{\mu})$ as a function of energy for protons (○) and iron (▲). The two species are almost indistinguishable as desired for an energy parameterization. Over 900 proton and 900 iron vertical showers are included.

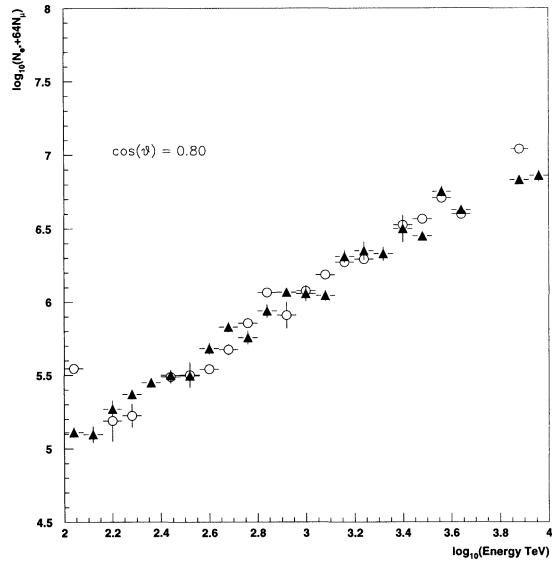

Fig. 4. Energy parameterization as in Fig. 3, except here for inclined showers ($\cos\theta = 0.8$). The relation varies slightly with zenith angle (here, $\log 10(N_{e*} + 64 \times N_{\mu})$ is best), but remains insensitive to composition.

events (described in the next section as well as [10]). This parameterization is logarithmically linear with energy and insensitive to the primary particle type. The factor of 60 multiplying N_{μ} in this expression gives the most compositional insensitivity, though anything between about 55 and 65 would yield good results too. The best value increases slightly with zenith angle, reaching about 65 for a zenith angle of 45 degrees. As an illustration, Fig. 4 shows the best expression at a larger zenith angle ($N_{e*} + 64 \times N_{\mu}$), for data at $\cos\theta = 0.80$. Again, the parameterization is logarithmically linear with E and independent of composition. Similar relations are found to hold at all zenith angles to 45°.

The relative weighting of N_{μ} and N_{e*} suggests that the above parameterization is closely related to the total particle kinetic energy arriving at ground level. A typical muon energy at the ground is about 1 GeV, while electrons and photons are usually less than 20 MeV, due to their more significant energy losses from scattering in the air.

This method of energy determination yields systematic differences between the iron and proton energy assignments of less than 5%. The average absolute values of the energy reconstruction errors decreases from about 25% near 10^{14} eV to about 16% above 10^{15} eV.

Such compositional insensitivity is crucial to producing an accurate energy spectrum. That is, if the composition changes in some energy region of interest, then the relationship between measured electron size and inferred energy will also change. Without an independent means of assessing the composition, an energy spectrum determined from N_{e*} alone is subject to (unknown) systematic shifts. The weighted combination of N_{e*} and N_{μ} is a robust way of determining the energy without these systematic uncertainties.

6. The size spectrum

As a first step in assembling the cosmic ray energy spectrum from CASA-MIA data, size spectra are examined. The electron size related parameter N_{e*} is derived from the normalization of the fitted lateral distribution function of observed particle densities in the surface array. As such, N_{e*} has no dependence on models or simulations. Similar remarks pertain to the measured muon size N_{μ}. The fits are described in more detail in [10], and are shown to be well behaved for the purposes of generating a spectrum in [15].

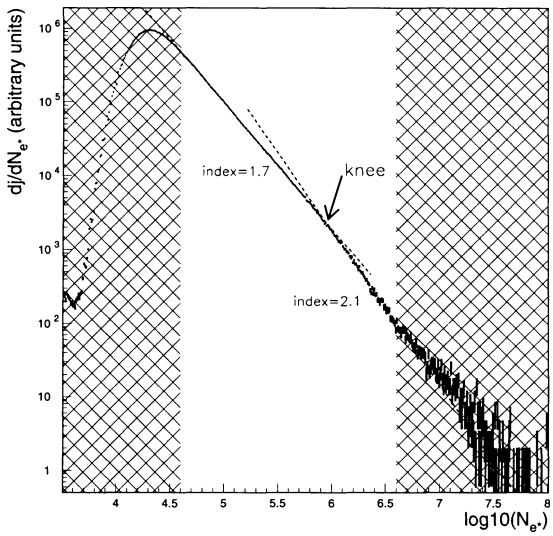

Fig. 5. The vertical cosmic ray N_{e*} spectrum from CASA-MIA. The error bars are statistical. Hatched regions are those in which the data are not reliable. The spectrum is a double power law $(dj/dN_{e*}) \propto N_{e*}^{-\gamma}$ with spectral indices of 1.69 ± 0.02 below the knee, and 2.12 ± 0.05 above (dashed lines). The knee is clearly visible around $10^{5.8}$ particles.

It is problematic to attempt to equate N_{e*} precisely to the number of electrons above some energy threshold in an air shower. N_{e*} actually represents a combination of electrons, positrons, and photons at ground level, owing to the thin lead sheets atop the CASA counters. The photon detection efficiency is small, but their numbers are abundant, so they contribute significantly to the signal. Thus, this size in not exactly the "proper" electron size, and it is prudent to use caution when comparing N_{e*} to size measurements reported by other experiments. Nevertheless, it is seen from simulation studies that N_{e*} is a robust fitted quantity which is approximately equal to the number of shower electrons above a few MeV.

Fig. 5 shows the vertical N_{e*} spectrum measured with CASA-MIA. Only events which arrived from within 14° of the zenith and within 150 m of the center of the array are included. The detector is seen to reach full efficiency around $10^{4.6}$ particles. Values of N_{e*} larger than $10^{6.6}$ particles are potentially prone to reconstruction error as the events begin to extend beyond the edge of the array, even if their cores are at the very center. In such large events, significant numbers of CASA stations may also become individually saturated. For these reasons, events whose fits result in sizes below full efficiency ($N_{e*} < 10^{4.6}$ particles) or above saturation ($10^{6.6}$ particles), denoted by the "hatched" region of Fig. 5, are not included in this analysis. This spectrum represents over 54 million events, over 12 million of which are in the acceptable region of N_{e*}. Of those rejected, about 2700 were above the upper cutoff point.

The differential N_{e*} spectrum in Fig. 5 appears as two power laws, each of the form

$$\frac{dN}{d\log N_{e*}} \propto {N_{e*}}^{-\gamma}, \tag{1}$$

with a spectral transition at a size of about $N_{e*} = 10^{5.8}$ particles. The spectral index γ is 1.69 ± 0.02 for sizes smaller than this, and 2.12 ± 0.05 for larger sizes. The dashed lines in Fig. 5 are the best fit power law equations (which are primarily visible here as they extend beyond the fitted points).

A good test of whether the observed knee of the spectrum is actually a characteristic of the underlying energy spectrum or, perhaps, a detector effect is to examine the N_{e*} spectrum at different zenith angles. Showers at different zenith angles have passed through different amounts of atmosphere, and thus are at different locations along their longitudinal development when measured at the ground. At some given primary energy, a shower from a larger zenith angle will have passed through more atmosphere and therefore will be diminished in size when compared to a similar shower which arrived from the vertical. If a feature in the size spectrum appears at the same size regardless of zenith angle, then it is likely a detector effect (such as an error in the size fitting routines) and is not necessarily indicative of a corresponding feature in the energy spectrum. On the other hand, a feature in the size spectrum which *does* move to smaller sizes with increasing zenith angle suggests that it may be a feature in the energy spectrum, though certain detector effects could mimic this as well.

Fig. 6 shows N_{e*} spectra at several angles from CASA-MIA data. The points shown overlaying the data are given to indicate the location of a spectral change. They are derived from fitting the data to two power laws, each with a distinct spectral index, joined at the position shown by the point. The fit was performed such that the location of the spectral break, as well as the normalizations and slopes of the two

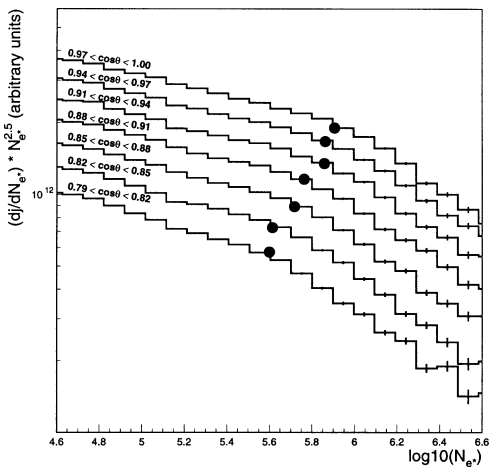

Fig. 6. The cosmic ray N_{e*} spectrum at various angles. To better display the knee, the spectrum was multiplied by $N_{e*}^{2.5}$. Labels indicate the range of zenith angles from which showers were accepted for each histogram. Points show the location of the knee from double power law fits.

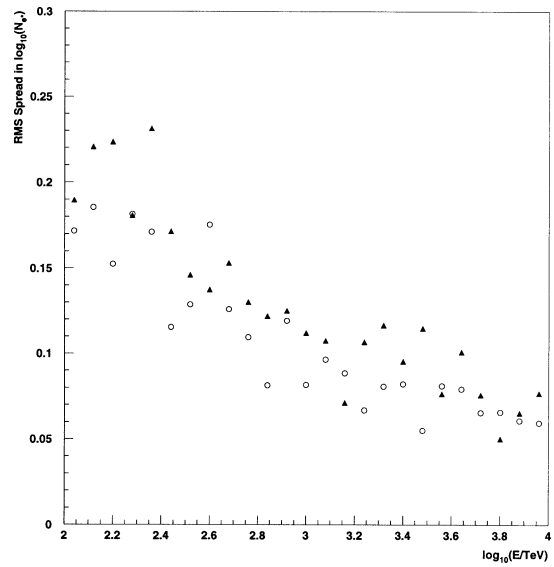

Fig. 7. The r.m.s. spread in reconstructed $\log_{10} N_{e*}$, from simulated iron (▲) and proton (○) showers. This spread includes both intrinsic size fluctuations and reconstruction errors. The accuracy improves with energy and displays no unusual systematic effects related to composition. The relative size error, estimated the graph (see text), is less than 25% in the vicinity of the knee.

power laws on either side of it, were all simultaneously allowed to vary until a best fit was found. The displayed points are thus accurately reflecting the location of the break (or "knee"), which is seen to move to smaller N_{e*} with increasing zenith angle. The indicated change-points are useful for comparison to one another, but are systematically slightly different from change-points derived from other types of spectral fits (e.g., in the fits shown later in Fig. 10).

Detector or fitting systematics such as edge effects or systematic errors in reconstruction could possibly introduce a knee feature in the N_{e*} spectrum or cause the observed movement of the knee with zenith angle. Extensive studies have been performed to rule out these possibilities [15]. The intensity and shape of the spectrum are insensitive to the core-cut used in data selection. The largest showers studied are neither saturating the detector nor extending beyond its boundaries in a way to produce misfits of shower size.

Fig. 7 exhibits the r.m.s. spread in the reconstructed value of $\log_{10}(N_{e*})$ as a function of energy for simulated iron and proton events. This spread includes reconstruction errors and the intrinsic size fluctuation of the events. The combination of both sources of uncertainty is necessary to assess their potential influence on the shape of the size spectrum. The variance decreases smoothly with energy, showing no systematic anomalies in the knee region. No significant composition dependence is apparent. The magnitude of the errors are insufficient to cause a sharp change in the size spectrum [15]. Similar remarks apply to the muon reconstruction; studies of the net error in energy reconstruction are described in the next section.

The relative size uncertainty can be estimated from Fig. 7 by multiplying by 2.30. For example, near 10^{15} eV, the spread is about 10%, corresponding to $\Delta N_{e*}/N_{e*} \approx 23\%$. A significant portion of this is due to intrinsic fluctuations.

In summary, the change in the slope of the size spectrum is not due to detector effects or systematic errors. Its change with zenith angle is strong *simulation independent* evidence that the observed knee is a feature of the parent energy spectrum.

7. The energy spectrum

Using the energy relationship derived in Section 5, Fig. 8 shows the energy spectrum for vertical cosmic ray showers. Table 1 contains several values from this histogram. As in the previous section, a core cut of

Table 1
Measured differential energy spectrum (vertical data)

$\log_{10}(E, \text{TeV})$	$dj/dE \times E$ (m^{-2} sec^{-1} sr^{-1})
2.2	$(4.94 \pm 0.02) \times 10^{-5}$
2.3	$(3.32 \pm 0.02) \times 10^{-5}$
2.4	$(2.29 \pm 0.01) \times 10^{-5}$
2.5	$(1.56 \pm 0.01) \times 10^{-5}$
2.6	$(1.08 \pm 0.01) \times 10^{-5}$
2.7	$(7.13 \pm 0.07) \times 10^{-6}$
2.8	$(4.89 \pm 0.06) \times 10^{-6}$
2.9	$(3.43 \pm 0.05) \times 10^{-6}$
3.0	$(2.27 \pm 0.04) \times 10^{-6}$
3.1	$(1.41 \pm 0.03) \times 10^{-6}$
3.2	$(9.8 \pm 0.3) \times 10^{-7}$
3.3	$(6.1 \pm 0.2) \times 10^{-7}$
3.4	$(4.0 \pm 0.2) \times 10^{-7}$
3.5	$(2.5 \pm 0.1) \times 10^{-7}$
3.6	$(1.5 \pm 0.1) \times 10^{-7}$
3.7	$(9.6 \pm 0.8) \times 10^{-8}$
3.8	$(6.3 \pm 0.7) \times 10^{-8}$
3.9	$(4.8 \pm 0.6) \times 10^{-8}$
4.0	$(2.9 \pm 0.4) \times 10^{-8}$

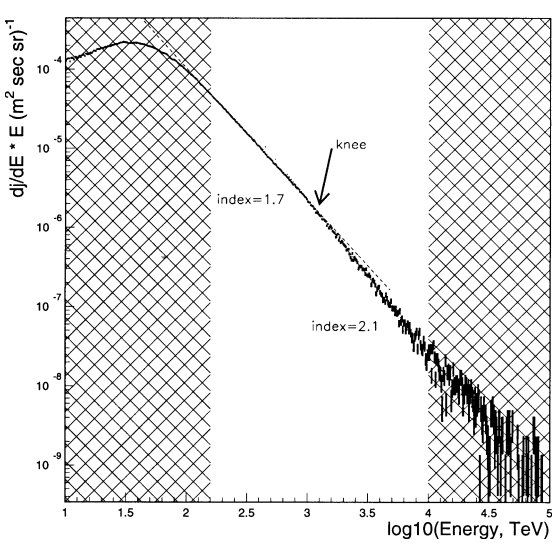

Fig. 8. The vertical cosmic ray energy spectrum. The error bars are statistical. Hatched areas are those in which the data may be subject to detector effects. The spectrum is a double power law ($dj/d\log E$) $\propto E^{-\gamma}$ with indices of 1.66 ± 0.02 below the knee and 2.00 ± 0.05 above (dashed lines). The knee is clearly visible around 10^3 TeV. (Error bars represent statistical errors only. Systematic effects due to reconstruction errors are not shown.)

150 meters and a zenith angle cut of 14° are included. Over 35 million events appear in the spectrum, with over 4 million of these above full efficiency and below whole detector saturation. (The hatched regions in Fig. 8 denote energies below full efficiency or above whole detector saturation which are not used in further analysis. These constant energy cuts roughly correspond to the location of the cuts in the N_{e*} spectrum.) Another 10 million events were assigned energies below 10 TeV and do not appear in the figure. The total data examined for the vertical energy spectrum is roughly equal to that of the vertical N_{e*} spectrum. The fraction of events falling in the acceptable region is lower than for the N_{e*} spectrum because of the detector's composition dependent threshold. A shower from a light primary will generate more particles at the ground than a shower from a heavier particle of the same energy. So more low energy proton events than iron showers will trigger the detector. The region over which the detector is not fully efficient spreads due to this compositional effect.

As was the case for the N_{e*} spectrum, the differential energy spectrum displays a knee feature, near an energy of 10^{15} eV. The energy spectrum is seen to have a power law form

$$\frac{dN}{d\log E} \propto E^{-\gamma}, \tag{2}$$

with spectral indices of 1.69 ± 0.02 below the knee and 2.07 ± 0.05 above. These are denoted by dashed lines in Fig. 8, which are mainly seen as they extend beyond the fitted points. Correcting these numbers for the systematics introduced by the combination of energy error, binning, and the steep spectrum gives indices of 1.66 ± 0.02 and 2.00 ± 0.05 (see [15] for details).

To further support the interpretation that the observed bend is a feature of the energy spectrum, Fig. 9 shows the spectra for several different angles. To more clearly show that the position of the knee does not change with zenith angle, all spectra were multiplied by $E^{2.5}$ and an arbitrary factor to bring them out of vertical alignment for display purposes. The circles represent the location of the knee according to a double power law fit as performed for the N_{e*} spectrum in Fig. 6. Its location does not change significantly with zenith angle.

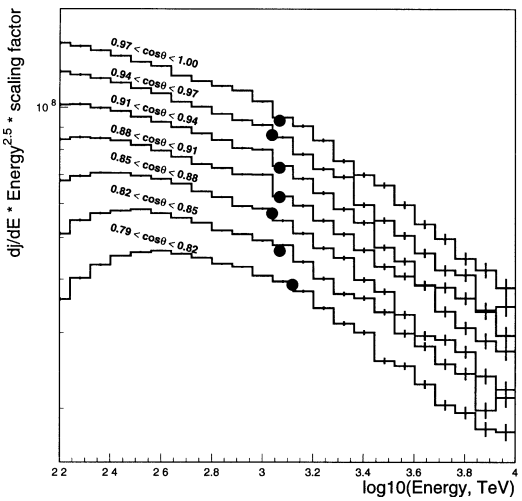

Fig. 9. The cosmic ray energy spectrum at various angles. In each case, the number of events was multiplied by a factor to bring the spectra out of vertical alignment so the behavior of the knee can be seen. The location of the knee, represented by the circles, is constant with zenith angle. (Error bars represent statistical errors only. Systematic effects due to reconstruction errors are not shown.)

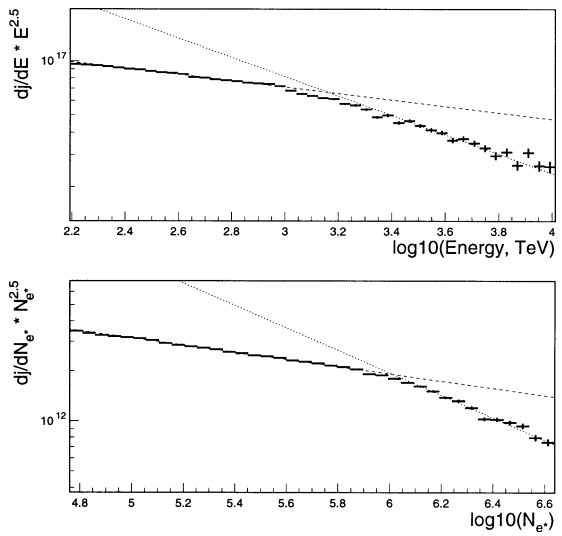

Fig. 10. A closer look at the knee. The energy spectrum (top) does not appear to have a single break, but a transition occurring over a range of energies. The N_{e*} spectrum (bottom) has a sharper break. (In the upper graph, $dj/dE * E^{2.5}$ is given in $\mathrm{eV}^{1.5}/(\mathrm{m}^2\ \mathrm{sec\ sr})$, and in the lower, dj/dN_{e*}, is given in arbitrary units.) Note that the fits used here differ from those done for Fig. 6, so the location of the intersection of the two power laws above differs slightly from the indicated "break" points in Fig. 6.

The absolute intensity of the cosmic ray flux at zenith angles other than vertical vary by less than 8% from the values given in Table 1 in the knee region. No systematic variation is seen with zenith angle.

As described in the previous section for the size spectrum, systematic errors or detector effects are ruled out as causing the knee itself. Moreover, studies have been carried out to investigate whether the smoother steepening change of the energy spectrum when compared to the size spectral knee could possibly arise from such errors [15]. Among these studies are the following: (i) The single-power-law relation, nearly linear, between the energy parameter and primary energy (recall Figs. 3 and 4) shows no systematic shifts with energy. (ii) The energy spectrum's shape and intensity have no zenith angle dependence. (iii) The error in energy reconstruction is modest (see Section 5), is independent of composition assumptions, and smoothly improves with energy. Studies of artificially generated spectra smeared by the measured resolution function do not significantly alter the shape of those spectra.

8. The knee

With an accurate, compositionally independent all particle spectrum, the question of the sharpness of the knee of the cosmic ray energy spectrum observed by previous experiments can be addressed. Fig. 10 shows a more detailed view of the knee in both the energy spectrum and the N_{e*} spectrum as measured by CASA-MIA. The change in spectral index of the energy spectrum does not appear to be sharp, but rather to undergo a transition over the range of energies 10^{15} eV to $10^{15.4}$ eV. The N_{e*} spectrum, in contrast, undergoes a sharper change.

The dashed lines in Fig. 10 show fits of single power laws, done separately on data well above and well below the knees in both the size and the energy plots. Their intersections are shown only to help qualitatively gauge the "sharpness" of the transition of the measured data spectra. Since these fits differ from those described earlier (Sections 6 and 7; Figs. 6 and 9), the intersections do not correspond to the break-points given there.

Further understanding of the situation can be gained

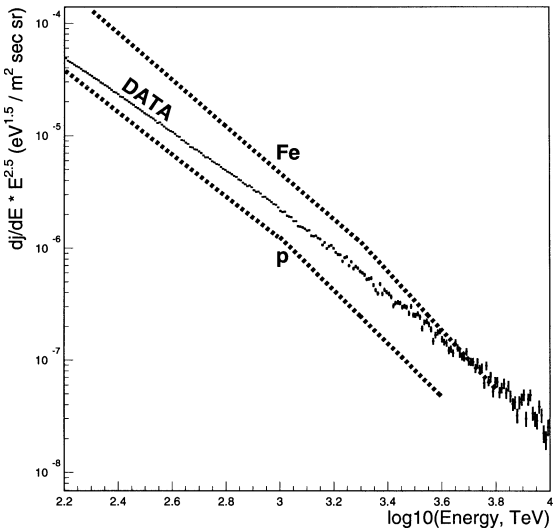

Fig. 11. The calculated energy spectrum compared to the spectrum which would have resulted from computing energies based only on N_{e*} and an assumed composition. (Shown for pure iron and pure proton assumptions.)

from Fig. 11. The energy spectrum obtained from data is shown, as well as dashed lines which represent the energy spectrum which would have been obtained had the energy been computed using N_{e*} *only* (i.e., using *no* muon information). The relationship between N_{e*} and E is dependent on assumptions made about the nuclear type of the primary, so two such curves are shown, one assuming the particles are entirely protons, and the other for pure iron. Each of these curves was obtained by converting the observed N_{e*} spectrum to an energy spectrum using formulae obtained from studies of simulated events,

$$\log_{10}(E) = 1.03 \times \log_{10}(N_{e*}) - 3.19 \quad \text{for protons,} \tag{3}$$

$$\log_{10}(E) = 0.81 \times \log_{10}(N_{e*}) - 1.56 \quad \text{for iron.} \tag{4}$$

The energy spectra converted from N_{e*} spectra are only drawn over the ranges of energies which correspond to reliable N_{e*} spectrum measurements. If cosmic rays were in fact purely protons, then our observed spectrum should overlap the dashed curve labeled "p"; if the data were all iron, its curve would coincide with the "Fe" line. A mixed composition which does not change with energy would lie between these curves and have the same shape and slopes.

When viewed in this way in Fig. 11, the data suggest a change of composition from light to heavy over this energy range. The details are more thoroughly addressed in [15] and will be the topic of a forthcoming paper [16]. A smooth rolling over of the energy spectrum can become a sharper break in the N_{e*} spectrum if the composition is becoming heavier (with corresponding smaller shower sizes). Indeed, this effect could arise if the smooth energy knee in the observed all-particle spectrum is the sum of several sharper breaks found in the spectra of individual component species. While supernova acceleration and galactic escape models predict that higher mass species should exhibit a spectral change or cutoff at higher energy (proportional to their charge Z), these heavier species would also register smaller shower sizes on the ground than their equal energy but lower mass counterparts. This would tend to allow various spectral breaks from several nuclear species to more closely align in measured size, causing a much sharper break in the size spectrum than observed in the energy spectrum.

The smoothness of the transition in the energy spectrum seen here is in contrast with some previous observations [1,3], for example those of the Akeno group [5]. This is a very interesting result, as the sharpness of the knee of the cosmic ray spectrum has been a fundamental source of problems for theories attempting to explain it. Moreover, the sharpness of the N_{e*} spectrum's knee measured by CASA-MIA is evidence that the sharpness observed in some of the previous energy spectrum measurements which were derived from electron size could have originated in a compositional change in this region.

9. Comparing with the Tibet Air Shower Array

The Tibet Air Shower Array group has also seen a smooth knee in the energy spectrum [4]. The high altitude of the Tibet array allows measurements near shower maximum, where the size is less sensitive to composition than at lower altitudes.

The spectrum as measured with the Tibet array [4] and the Akeno array [5] are compared to the CASA-MIA result in Fig. 12. Both the absolute intensity of the flux and the location of the knee in the spectrum appear to be slightly different. However, the majority of the visually dramatic difference in the figure is at-

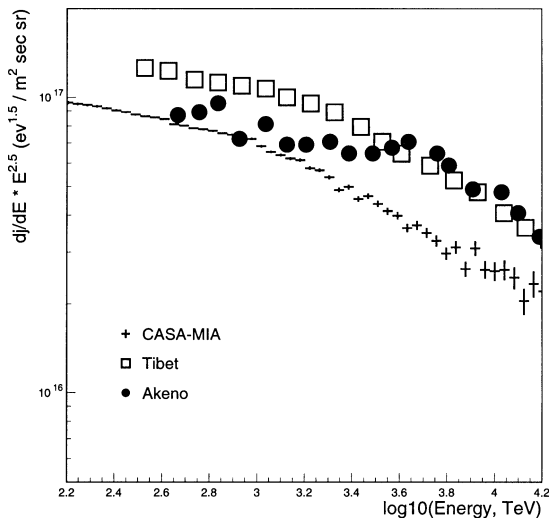

Fig. 12. The CASA-MIA experiment compared to Tibet and Akeno. The observed differences are likely due primarily to how each experiment's simulation assigns energies (see Fig. 13). The Tibet and Akeno results are from [4] and [5], respectively.

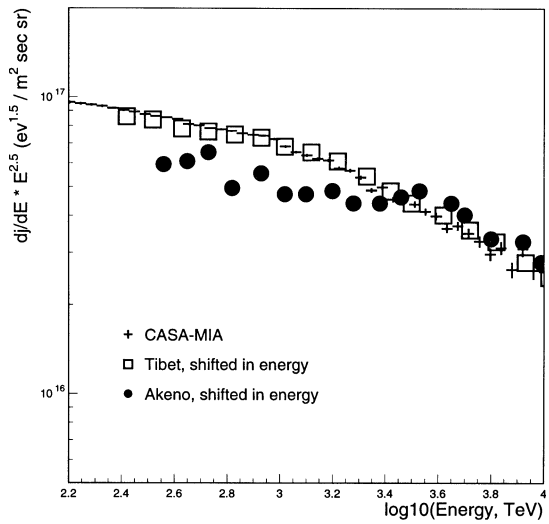

Fig. 13. The CASA-MIA experiment compared to energy shifted Tibet and Akeno results. The reported Tibet and Akeno results are presented here after decreasing each data point's energy by about 20%. The close agreement between CASA-MIA and Tibet as to the shape of the knee is apparent. (Tibet and Akeno results are from [4] and [5], respectively.)

tributable to the factor of $E^{2.5}$ by which the spectra are multiplied. This factor magnifies differences, in particular those between the energies assigned by the different experiments and their simulations. Fig. 13 shows the Tibet and Akeno spectra after their energy scales are each modestly shifted down by 20% of their reported values (i.e., $\delta \log E = -0.11$). Such a shift in energy moves each curve both down and to the left in the plot. The differences in the Tibet and Akeno magnitudes between this figure and the previous one are *only* due to the energy shift and related $E^{2.5}$ factor. The agreement between CASA-MIA and these results is now much more obvious – the majority of the discrepancy observed in Fig. 12 is possibly due to a systematic difference between the simulations used in each case to assign energy. Note also that the *shape* of the energy spectra are unaffected by the uniform energy shift.

The Tibet group used a different simulation from that used in this work and applied it at a different altitude. The required energy shift (20%) is relatively small – about the size of the statistical uncertainty in energy assignment due to shower fluctuations. These differences could easily account for an energy shift of this magnitude.

With the above energy shift, the entirely independent Tibet and CASA-MIA results agree quite well. CASA-MIA's ability to reproduce the sharp break when using a compositionally *sensitive* method of examining the spectrum, and produce a smooth knee when using a compositionally *insensitive* one (recall Fig. 11), is evidence that compositional factors or detector effects may have played a major, unaccounted for role in previous measurements.

10. Conclusions

CASA-MIA observes a smooth spectral chance ("knee") in the cosmic ray primary energy spectrum, a feature which does not arise from detector effects. This spectrum is obtained using an energy reconstruction algorithm which is insensitive to the type of primary cosmic ray particle. Sharper spectral changes would result from the use of algorithms which do depend on assumptions about the nature of the primaries. A comparison of spectra obtained in these two ways suggests that the composition is becoming heavier with energy. Both the shape of the energy spectrum and the apparent composition change are consistent with a supernova shock wave model of cosmic ray acceleration with either the source turning

off or with cosmic ray escape from the galaxy. While the CASA-MIA results cannot distinguish between these models, they can exclude models which predict a sharp knee in the spectrum or a mass composition which becomes lighter with energy through the knee.

Acknowledgements

The authors gratefully acknowledge the assistance of the Command and Staff of the U.S. Army Dugway Proving Grounds. We express thanks to M. Cassidy for technical support at Dugway, and acknowledge the contributions of A. Borione, K. Gibbs, and L. Rosenberg during the construction and initial operations of CASA-MIA. We also thank S. Golwala, M. Galli, J. He, H. Kim, L. Nelson, M. Oonk, M. Pritchard, K. Riley, P. Rauske, and Z. Wells for help in the data processing. This work is supported in part by the National Science Foundation and the Department of Energy. Some authors wish to acknowledge the support of the Rackham Graduate School at the University of Michigan, the Grainger Foundation, and the Alfred P. Sloan Foundation. CEC is a Cottrell Scholar of the Research Corporation.

References

[1] P. Sokolsky, Introduction to Ultrahigh Energy Cosmic Ray Physics (Addison-Wesley, Redwood City, CA, 1989).
[2] G.V. Kulikov, G.B. Khristiansen, Soviet Physics JETP 35 (1959) 441.
[3] A.A. Watson, Proc. 25th Int. Cosmic Ray Conference, Durban 8 (1997) 257.
[4] M. Amenomori et al., Ap. J. 461 (1996) 408.
[5] M. Nagano et al., J. Phys. G 10 (1984) 1295.
[6] Presentations at the International Symposium on Extremely High Energy Cosmic Rays: Astrophysics and Future Observatories, Tokyo (1996).
[7] The EAS-TOP Collaboration, Proc. 25th Int. Cosmic Ray Conference, Durban 4 (1997) 125.
[8] M. Roth et al., Proc. 25th Int. Cosmic Ray Conference, Durban 4 (1997) 157.
[9] J. Cortina et al., Proc. 25th Int. Cosmic Ray Conference, Durban 4 (1997) 69.
[10] A. Borione et al., Nucl. Instrum. Methods A 346 (1994) 329.
[11] K. Greisen, Ann. Rev. Nucl. Sci 10 (1960) 63.
[12] K. Greisen, Progress in Elementary Particle and Cosmic Ray Physics III (1956) 3.
[13] A.M. Hillas, Proc. 19th International Cosmic Ray Conference, La Jolla 1 (1985) 155.
[14] R.S. Fletcher et al., Phys. Rev. D 50 (1994) 5710.
[15] M.A.K. Glasmacher, Cosmic Ray Composition Studies with CASA¡MIA, Ph.D. thesis, The University of Michigan (1998).
[16] M.A.K. Glasmacher et al., in preparation (1998).